SCIENCE CHINA
Information Sciences

• RESEARCH PAPER •

April 2026, Vol. 69, Iss. 4, 142201:1–142201:17
https://doi.org/10.1007/s11432-025-4621-1

Substabilization for coupled-inverted pendulums with input failure: a fully actuated system approach

Guangren DUAN[1,2*], Liyao HU[1], Shiyu ZHANG[1], Zhijun CHEN[1] & Lin LIU[1]

[1]*Center for Control Theory and Guidance Technology, Harbin Institute of Technology, Harbin 150001, China*
[2]*Guangdong Provincial Key Laboratory of Fully Actuated System Control Theory and Technology, Southern University of Science and Technology, Shenzhen 518055, China*

Received 4 May 2025/Revised 17 August 2025/Accepted 27 September 2025/Published online 15 January 2026

Abstract This paper investigates the substabilization problem for a class of coupled-inverted pendulum systems (CIPSs) connected by two springs. Unlike most control studies that only focus on the CIPS without any input failure, this paper considers a more complex situation. That is, individual control inputs in the CIPS fail entirely, significantly complicating the control design. To solve this control problem, the original CIPS is converted into a sub-fully actuated system (sub-FAS) model. Then, using the fully actuated system (FAS) approach, the substabilizing controllers for the obtained sub-FAS are designed within the feasible set, and the corresponding region of exponential attraction (RoEA) is derived, in which the closed-loop sub-FAS is exponentially stable, and the original CIPS is asymptotically stable. Finally, simulation research proves the effectiveness of the proposed control method.

Keywords fully actuated system approach, substability and substabilization, pendulum systems, input failure

Citation Duan G R, Hu L Y, Zhang S Y, et al. Substabilization for coupled-inverted pendulums with input failure: a fully actuated system approach. Sci China Inf Sci, 2026, 69(4): 142201, https://doi.org/10.1007/s11432-025-4621-1

1 Introduction

Nonlinear control has been widely recognized as one of the most active research fields because of its application value. Until now, most experts and scholars have been inclined to tightly combine with the first-order state-space approaches to solve nonlinear control problems because the approaches have successfully addressed the control problems for linear time-invariant systems, raising many state-oriented dilemmas [1]. Furthermore, when modeling systems, due to the use of a series of physical laws, the original models of many physical systems are second- or high-order ones. Thus, if we use the approaches to design controller, it is inevitable to convert the original system into first-order ones by reducing the system order. However, this procedure will increase the system dimensions and destroy the full-actuation feature of the system. In fact, the state-space approaches are more suitable for solving the problems of response analysis and state observer design, and do not provide enough convenience for system controller design [1]. Fortunately, in recent years, Duan heuristically proposed the high-order fully actuated system (HOFAS) models together with a control-oriented approach, namely, the fully actuated system (FAS) approach [1,2]. Different from the state-space approach, using the FAS approach can fully utilize the full-actuation feature of system, and thus directly design controller for nonlinear high-order systems, which significantly simplifies control design. Furthermore, in certain situations, a linear closed-loop system can be obtained with an arbitrarily desired eigenstructure. The reader is referred to [2] and its relevant studies for a detailed discussion about the FAS approach. At present, vast scientific research and engineering applications on the FAS approach have been widely reported relying on its inherent advantages in control design. Therein, some scholars focus on control research for systems with actuator or input failures, and have obtained numerous significant results. As a pioneering work, Cai et al. presented a fault tolerance framework for HOFASs with disturbances and multiplicative actuator faults, and firstly introduced the extended state observer into HOFASs [3]. In addition, a simpler case, namely, the scalar system, was considered in [4]. Ulteriorly, to handle simultaneously parameter uncertainties, actuator faults, and measurement noises, a novel observer-based low-power fault tolerant control (FTC) was established in [5], which indeed filled the relevant gaps in the safety control of FASs. Very recently, Cai et al. also studied the FTC for unknown nonaffine HOFASs with multiplicative actuator and sensor faults, concluding that the ultimately

* Corresponding author (email: g.r.duan@hit.edu.cn)

uniformly bounded stability was achieved [6]. For a more general system that can be decomposed into a fully actuated subsystem and an extra autonomous subsystem, a fault-tolerant controller was constructed to ensure the stabilization of such compound systems with nonlinear uncertainties and actuator faults, relying on the theory of input-to-state stability [7]. In applications, Ma et al. developed the prescribed-time and neuroadaptive cooperative FTC for heterogeneous multiagent systems subject to partial effectiveness loss faults in [8,9], respectively. However, most existing studies for systems with actuator or input failures focus primarily on the scenarios involving partial actuator or input failures, while more extreme cases, such as entire actuator or control input failures, have received relatively little attention, possibly due to the significantly greater complexity of control design for such systems. However, these scenarios are commonly observed in practical engineering applications.

The control for inverted pendulums is a typical problem in the control community, and various relevant control methods have been proposed [10–14]. In [11], a control strategy based on an energy method was proposed for trolley and pendulum systems. Different from the inverted pendulum without uncertainties considered in [11], the control problem for inverted pendulums with uncertainty was further considered in [12–14]. Therein, in [12], an output feedback stabilization method was developed to ensure that the equilibrium point of the closed-loop system is exponentially stable. In [13], an interval type-2 fuzzy PID control method was proposed for a cart-pendulum system with an uncertain model. In [14], a backstepping-based sliding mode control method was presented for uncertain underactuated systems and was further validated on cart-pendulum systems. Along this line of research, a few studies consider more complicated coupled-inverted pendulum systems (CIPSs). For example, a CIPS connected by a spring was studied in [15], for which a combined nonlinear control method using the hyperstability criterion was proposed. In addition, the decentralized control methods were presented in [16–18], and were successfully applied to the stabilization control for CIPSs. Under the framework of the FAS approach, there are also some references that focus on the control research for inverted pendulums [19, 20]. In [19], an adaptive guaranteed cost tracking control method was proposed for FASs with unknown parameters and applied to the guaranteed cost control for an inverted pendulum. Different from [19], in [20], the practical prescribed time control method for a class of strongly interconnected nonlinear systems was given, and verified on an inverted pendulum. Further, some scholars have investigated the control problems for inverted pendulum systems with actuator or input failures. In order to overcome the actuator faults, Ref. [21] proposed a sliding mode-based FTC method for a class of inverted pendulum and cart systems. Similarly, in [22], the adaptive fuzzy sliding mode control approach was developed against actuator faults. For a class of inverted pendulums with actuator faults and dead zones, Ref. [23] proposed a funnel-based neural adaptive FTC method. Ref. [24] solved the adaptive fuzzy tracking control problem for a class of double inverted pendulums with actuator failures. Based on the prescribed performance control and the FTC, Ref. [25] addressed the preassigned tracking performance problem for inverted pendulums with unknown control directions, actuator and component faults. The FTC scheme for sample-data systems was developed in [26] and subsequently applied to an inverted pendulum with floating faults. In [27], the disturbance observer-based robust control method was applied to a class of CIPSs with a stuck actuator, ensuring good output performance. Then, Ref. [28] extended the result of [27] to the decentralized control one for reducing information exchange among multiple inverted pendulum systems. In [29], the event-driven-observer-based adaptive distributed fault compensation control method was applied to the CIPSs with time-varying uncertainties and partial actuator loss faults. However, most of the aforementioned studies have focused only on some specific actuator or input failures, including but not limited to floating faults and partial loss faults. There is a lack of extensive research on cases involving entire input failures.

As a matter of fact, the FAS approach-based substabilization method can be invoked to address this circumstance. According to the definition of sub-FASs, Duan provided some new concepts, that is, substability and substabilization, which allow "gaps" and "holes" in the region of attraction of the Lyapunov exponential stability, and even allow the origin to be a boundary point of the region of attraction [30]. They are very useful, especially when the region of attraction could be large enough for certain applications. The reader is referred to the discussion about the sub-FASs, as detailed in [30]. Considering the case that a CIPS with full-actuation feature becomes underactuated due to individual control input failure, we can equivalently convert it into a sub-FAS with a nonempty feasible set, and thus design the substabilizing controllers and provide the corresponding region of exponential attraction (RoEA) with the help of the substabilization method. Therefore, in light of the above discussion, this paper investigates the substabilization problem for a class of CIPSs with individual input failure by using the FAS approach-based substabilization method. Main studies and contributions of this paper are as follows.

(1) The substabilization problem for the CIPS is addressed for the first time, which establishes a novel robust control framework for CIPS with input failure.

(2) Different from most prior studies focused on the control research for the CIPS without any failure or with partial actuator/input failures [26–29], this paper focuses on a more complex situation where individual control

inputs fail entirely. In this scenario, we can only design the remaining controllers to achieve the stability of the whole CIPS, which is a challenging task that constitutes the primary innovation of this paper.

(3) For control design, the original CIPSs are transformed into the sub-FAS models, based on which the sub-stabilizing controllers are designed within the feasible sets. Furthermore, the corresponding RoEAs are derived, in which the exponential stability of the closed-loop sub-FASs and the asymptotic stability of the original CIPSs are ensured.

The remainder of this paper is organized as follows. The problem formulations are given in Section 2. Some useful preliminaries are provided in Section 3. Sections 4 and 5 give respectively the control design for the CIPS with two different situations. The simulation research is shown in Section 6 to prove the effectiveness of our control method. Finally, the conclusion appears in Section 7.

Notations. In the following sections, let $f^{(k)}(t)$ denote the k-th derivative of the function $f(t)$ and $\bar{s}$ denote the complex conjugate of the complex number $s \in \mathbb{C}$. For a variable $\theta \in \mathbb{R}$, let

$$\theta^{(0\sim k)} = \begin{bmatrix} \theta \\ \dot{\theta} \\ \vdots \\ \theta^{(k)} \end{bmatrix}, \tag{1}$$

$$\boldsymbol{A}^{0\sim m-1} = \begin{bmatrix} a_0 & a_1 & \cdots & a_{m-1} \end{bmatrix}, \tag{2}$$

and

$$\boldsymbol{\Phi}\left(\boldsymbol{A}^{0\sim m-1}\right) = \begin{bmatrix} 0 & 1 & & \\ \vdots & & \ddots & \\ 0 & 0 & \cdots & 1 \\ -a_0 & -a_1 & \cdots & -a_{m-1} \end{bmatrix} \in \mathbb{R}^{m\times m}, \tag{3}$$

where k, $m \in \mathbb{Z}^+$, $a_i \in \mathbb{R}$, $i = 0, 1, \cdots, m-1$ are a set of proper constants.

2 Problem descriptions

Consider a class of CIPSs depicted in Figure 1 [18], of which the dynamic equation is shown as follows:

$$S: \begin{cases} S_1: \ddot{\theta}_1 = \frac{g}{l}\sin\theta_1 + \frac{k_1 a^2}{m_1 l^2}(\sin\theta_2\cos\theta_2 - \sin\theta_1\cos\theta_1) + u_1, \\ S_2: \ddot{\theta}_2 = \frac{g}{l}\sin\theta_2 + \frac{k_1 a^2}{m_2 l^2}(\sin\theta_1\cos\theta_1 - \sin\theta_2\cos\theta_2) + \frac{k_2 a^2}{m_2 l^2}(\sin\theta_3\cos\theta_3 - \sin\theta_2\cos\theta_2) + u_2, \\ S_3: \ddot{\theta}_3 = \frac{g}{l}\sin\theta_3 + \frac{k_2 a^2}{m_3 l^2}(\sin\theta_2\cos\theta_2 - \sin\theta_3\cos\theta_3) + u_3, \end{cases} \tag{4}$$

where θ_i, $i = 1, 2, 3$ are the angles of the i-th pendulum (°), u_i are the corresponding control inputs (N/(kg·m)). Furthermore, m_i, $i = 1, 2, 3$ are the mass of the i-th rod (kg), k_1 and k_2 are the spring constants (N/m), g is the gravitational acceleration (m/s^2), l and a are, respectively, the length of each rod and the distance from the pivot to the center of gravity of the rod (m).

For system (4), this paper considers two special situations where u_1 and u_2 entirely fail, respectively, which often occur in real-world systems.

2.1 The CIPS with the failed input u_1

First, we consider the first situation, in which the control input u_1 fails entirely. Then, the original system (4) is changed into

$$S_\alpha: \begin{cases} S_1: \ddot{\theta}_1 = \frac{g}{l}\sin\theta_1 + \frac{k_1 a^2}{m_1 l^2}(\sin\theta_2\cos\theta_2 - \sin\theta_1\cos\theta_1), \\ S_2: \ddot{\theta}_2 = \frac{g}{l}\sin\theta_2 + \frac{k_1 a^2}{m_2 l^2}(\sin\theta_1\cos\theta_1 - \sin\theta_2\cos\theta_2) + \frac{k_2 a^2}{m_2 l^2}(\sin\theta_3\cos\theta_3 - \sin\theta_2\cos\theta_2) + u_2, \\ S_3: \ddot{\theta}_3 = \frac{g}{l}\sin\theta_3 + \frac{k_2 a^2}{m_3 l^2}(\sin\theta_2\cos\theta_2 - \sin\theta_3\cos\theta_3) + u_3. \end{cases} \tag{5}$$

Problem 1. For the system (5), design two controllers u_2 and u_3, such that the closed-loop system (5) is asymptotically stable.

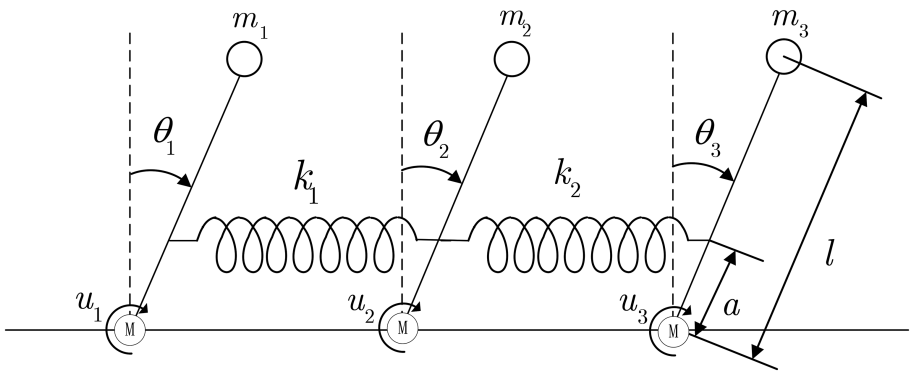

Figure 1 Coupled-inverted pendulums.

2.2 The CIPS with the failed input u_2

Then, we consider the second situation, in which the control input u_2 fails entirely. Then, the original system (4) is changed into

$$S_\beta : \begin{cases} S_1 : \ddot{\theta}_1 = \frac{g}{l}\sin\theta_1 + \frac{k_1 a^2}{m_1 l^2}\left(\sin\theta_2\cos\theta_2 - \sin\theta_1\cos\theta_1\right) + u_1, \\ S_2 : \ddot{\theta}_2 = \frac{g}{l}\sin\theta_2 + \frac{k_1 a^2}{m_2 l^2}\left(\sin\theta_1\cos\theta_1 - \sin\theta_2\cos\theta_2\right) + \frac{k_2 a^2}{m_2 l^2}\left(\sin\theta_3\cos\theta_3 - \sin\theta_2\cos\theta_2\right), \\ S_3 : \ddot{\theta}_3 = \frac{g}{l}\sin\theta_3 + \frac{k_2 a^2}{m_3 l^2}\left(\sin\theta_2\cos\theta_2 - \sin\theta_3\cos\theta_3\right) + u_3. \end{cases} \tag{6}$$

Problem 2. For the system (6), design two controllers u_1 and u_3, such that the closed-loop system (6) is asymptotically stable.

3 Preliminaries

To facilitate subsequent discussion, some preliminaries are presented below.

The so-called FAS, introduced in [31], appears in the following form:

$$\boldsymbol{x}^{(n)} = \boldsymbol{f}\left(\boldsymbol{x}^{(0\sim n-1)}, t\right) + \boldsymbol{B}\left(\boldsymbol{x}^{(0\sim n-1)}, t\right)\boldsymbol{u}, \tag{7}$$

where $n \geqslant 1$ is an integer, $\boldsymbol{x} \in \mathbb{R}^r$ and $\boldsymbol{u} \in \mathbb{R}^r$ are, respectively, the state vector and the control input, $\boldsymbol{f}\left(\boldsymbol{x}^{(0\sim n-1)}, t\right) \in \mathbb{R}^r$ and $\boldsymbol{B}\left(\boldsymbol{x}^{(0\sim n-1)}, t\right) \in \mathbb{R}^{r\times r}$ are two piece-wise continuous matrix functions. Furthermore, as defined in [31], the sets of singularity and feasibility of system (7) are

$$\mathbb{S} = \{\boldsymbol{X} \,|\, \det \boldsymbol{B}(\boldsymbol{X}, t) = 0 \text{ or } \infty,\ \boldsymbol{X} \in \mathbb{R}^{nr}, t \geqslant 0\}, \tag{8}$$

and

$$\mathbb{F} = \mathbb{R}^{nr} \setminus \mathbb{S}, \tag{9}$$

respectively.

Definition 1 ([31])**.** The FAS (7) is called a sub-FAS when $\mathbb{S} \neq \emptyset$ or equivalently $\mathbb{F} \neq \mathbb{R}^{nr}$.

Consider the following time-varying nonlinear system:

$$\dot{\boldsymbol{x}} = \boldsymbol{f}(\boldsymbol{x}, t), \boldsymbol{f}(\boldsymbol{0}, t) = 0 \tag{10}$$

with $\boldsymbol{x} \in \mathbb{R}^r$ being the state vector. Without loss of generality, assume that system (10) possesses a unique equilibrium $\boldsymbol{x} = \boldsymbol{0}$.

Definition 2 ([30])**.** Let $\mathbb{Q} \subset \mathbb{R}^r$ be nonempty. If for any initial value $\boldsymbol{x_0} \in \mathbb{Q}$, the solution of system (10), $\boldsymbol{x}(t, \boldsymbol{x_0})$, exponentially converges to zero, then system (10) is called substable with respect to the RoEA $\mathbb{Q}$.

To present the definition of substabilization, further consider the following forced system:

$$\dot{\boldsymbol{x}} = \boldsymbol{f}(\boldsymbol{x}, t) + \boldsymbol{B}(\boldsymbol{x}, t)\boldsymbol{u} \tag{11}$$

with $\boldsymbol{u} \in \mathbb{R}^r$ being the control vector.

Definition 3 ([30])**.** The system (11) is called substabilizable if there are a nonempty set $\mathbb{Q} \in \mathbb{R}^r$ and a control vector $\boldsymbol{u} = \boldsymbol{\alpha}(\boldsymbol{x}, t)$, such that the closed-loop system

$$\dot{\boldsymbol{x}} = \boldsymbol{f}(\boldsymbol{x}, t) + \boldsymbol{B}(\boldsymbol{x}, t)\,\boldsymbol{\alpha}(\boldsymbol{x}, t) \tag{12}$$

is substable with respect to the RoEA $\mathbb{Q}$.

4 Substabilization for the CIPS (5)

This section focuses on the control design and analysis for the system (5) based on the FAS approach. First, we convert the system (5) into a sub-FAS. Then, for the obtained sub-FAS, the substabilizing controllers are designed, and the corresponding RoEA is derived.

4.1 Sub-FAS model of the CIPS (5)

In this subsection, the system (5) is converted into a sub-FAS for control design. First, from the subsystem S_1 of the system (5), we have

$$\theta_2 = \frac{1}{2}\arcsin\left(\frac{2m_1l^2}{k_1a^2}\left(\ddot{\theta}_1 - \frac{g}{l}\sin\theta_1\right) + \sin 2\theta_1\right) \tag{13}$$

and

$$\theta_1^{(3)} = \frac{g}{l}\dot{\theta}_1\cos\theta_1 + \frac{k_1a^2}{2m_1l^2}\left(2\dot{\theta}_2\cos 2\theta_2 - 2\dot{\theta}_1\cos 2\theta_1\right) \tag{14}$$

with the following constraint:

$$-1 \leqslant \frac{2m_1l^2}{k_1a^2}\left(\ddot{\theta}_1 - \frac{g}{l}\sin\theta_1\right) + \sin 2\theta_1 \leqslant 1. \tag{15}$$

Therefore, we have

$$\dot{\theta}_2 = \frac{\frac{m_1l^2}{k_1a^2}\left(\theta_1^{(3)} - \frac{g}{l}\dot{\theta}_1\cos\theta_1\right) + \dot{\theta}_1\cos 2\theta_1}{\cos\left(\arcsin\left(\frac{2m_1l^2}{k_1a^2}\left(\ddot{\theta}_1 - \frac{g}{l}\sin\theta_1\right) + \sin 2\theta_1\right)\right)} \tag{16}$$

with the second constraint:

$$\frac{2m_1l^2}{k_1a^2}\left(\ddot{\theta}_1 - \frac{g}{l}\sin\theta_1\right) + \sin 2\theta_1 \neq \pm 1. \tag{17}$$

From (5), (13) and (14), again taking the derivative for $\theta_1^{(3)}$, we obtain

$$\begin{aligned}\theta_1^{(4)} &= \frac{g}{l}\ddot{\theta}_1\cos\theta_1 - \frac{g}{l}\dot{\theta}_1^2\sin\theta_1 + \frac{k_1a^2}{m_1l^2}\ddot{\theta}_2\cos 2\theta_2 - \frac{2k_1a^2}{m_1l^2}\dot{\theta}_2^2\sin 2\theta_2 - \frac{k_1a^2}{m_1l^2}\ddot{\theta}_1\cos 2\theta_1 + \frac{2k_1a^2}{m_1l^2}\dot{\theta}_1^2\sin 2\theta_1\\ &= f_1\left(\theta_1^{(0\sim 3)}, \theta_3\right) + B_1\left(\ddot{\theta}_1, \theta_3\right)u_2,\end{aligned} \tag{18}$$

where

$$\begin{aligned}f_1\left(\theta_1^{(0\sim 3)}, \theta_3\right) &= \frac{g}{l}\ddot{\theta}_1\cos\theta_1 - \frac{g}{l}\dot{\theta}_1^2\sin\theta_1 + \frac{k_1a^2g}{m_1l^3}\sin\left(\frac{1}{2}\arcsin\left(\frac{2m_1l^2}{k_1a^2}\ddot{\theta}_1 - \frac{2m_1lg}{k_1a^2}\sin\theta_1 + \sin 2\theta_1\right)\right)\\
&\times\cos\left(\arcsin\left(\frac{2m_1l^2}{k_1a^2}\ddot{\theta}_1 - \frac{2m_1lg}{k_1a^2}\sin\theta_1 + \sin 2\theta_1\right)\right)\\
&+\frac{k_1^2a^4}{2m_1m_2l^4}\left(\sin 2\theta_1 - \frac{2m_1l^2}{k_1a^2}\ddot{\theta}_1 + \frac{2m_1lg}{k_1a^2}\sin\theta_1 + \sin 2\theta_1\right)\cos\left(\arcsin\left(\frac{2m_1l^2}{k_1a^2}\ddot{\theta}_1 - \frac{2m_1lg}{k_1a^2}\sin\theta_1 + \sin 2\theta_1\right)\right)\\
&+\frac{k_1k_2a^4}{2m_1m_2l^4}\left(\sin 2\theta_3 - \frac{2m_1l^2}{k_1a^2}\ddot{\theta}_1 + \frac{2m_1lg}{k_1a^2}\sin\theta_1 - \sin 2\theta_1\right)\cos\left(\arcsin\left(\frac{2m_1l^2}{k_1a^2}\ddot{\theta}_1 - \frac{2m_1lg}{k_1a^2}\sin\theta_1 + \sin 2\theta_1\right)\right)\\
&-\frac{2k_1a^2}{m_1l^2}\left(\frac{\frac{m_1l^2}{k_1a^2}\theta_1^{(3)} - \frac{m_1lg}{k_1a^2}\dot{\theta}_1\cos\theta_1 + \dot{\theta}_1\cos 2\theta_1}{\cos\left(\arcsin\left(\frac{2m_1l^2}{k_1a^2}\ddot{\theta}_1 - \frac{2m_1lg}{k_1a^2}\sin\theta_1 + \sin 2\theta_1\right)\right)}\right)^2\left(\frac{2m_1l^2}{k_1a^2}\ddot{\theta}_1 - \frac{2m_1lg}{k_1a^2}\sin\theta_1 + \sin 2\theta_1\right)\\
&-\frac{k_1a^2}{m_1l^2}\ddot{\theta}_1\cos 2\theta_1 + \frac{2k_1a^2}{m_1l^2}\dot{\theta}_1^2\sin 2\theta_1\end{aligned}$$

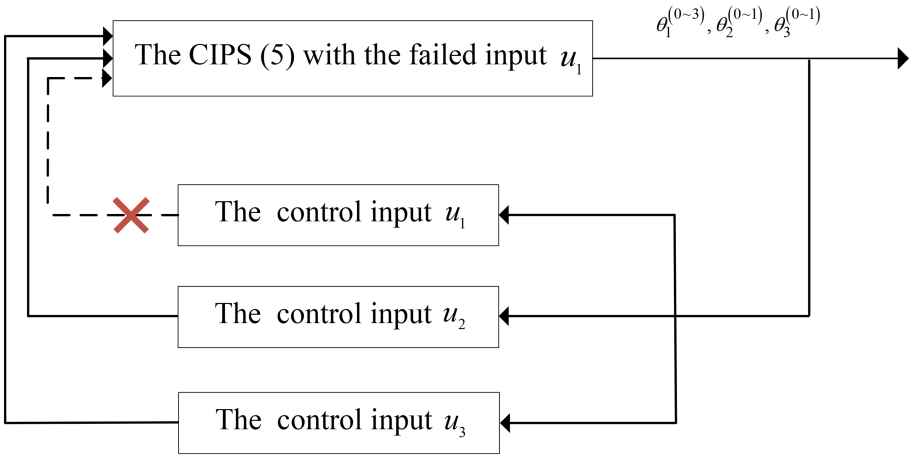

Figure 2 (Color online) The block diagram of the closed-loop system (5).

and

$$B_1\left(\theta_1, \ddot{\theta}_1\right) = \frac{k_1 a^2}{m_1 l^2} \cos\left(\arcsin\left(\frac{2m_1 l^2}{k_1 a^2}\left(\ddot{\theta}_1 - \frac{g}{l}\sin\theta_1\right) + \sin 2\theta_1\right)\right).$$

Furthermore, for subsystem S_3, according to (13), there is

$$\ddot{\theta}_3 = \tilde{f}_1\left(\theta_1, \ddot{\theta}_1, \theta_3\right) + u_3, \tag{19}$$

where

$$\tilde{f}_1\left(\theta_1, \ddot{\theta}_1, \theta_3\right) = \frac{g}{l}\sin\theta_3 + \frac{m_1 k_2}{m_3 k_1}\ddot{\theta}_1 - \frac{m_1 k_2 g}{m_3 k_1 l}\sin\theta_1 + \frac{k_2 a^2}{2m_3 l^2}\sin 2\theta_1 - \frac{k_2 a^2}{m_3 l^2}\sin\theta_3\cos\theta_3.$$

Thus, according to (18) and (19), we can obtain the corresponding sub-FAS model of the system (5) as follows:

$$\begin{bmatrix} \theta_1^{(4)} \\ \ddot{\theta}_3 \end{bmatrix} = \begin{bmatrix} f_1 \\ \tilde{f}_1 \end{bmatrix} + \begin{bmatrix} B_1 & 0 \\ 0 & 1 \end{bmatrix} \begin{bmatrix} u_2 \\ u_3 \end{bmatrix} \tag{20}$$

with the following feasible set:

$$\mathbb{F}_1 = \left\{ \begin{bmatrix} \theta_1^{(0\sim3)} \\ \theta_3^{(0\sim1)} \end{bmatrix} \middle| -1 < \frac{2m_1 l^2}{k_1 a^2}\left(\ddot{\theta}_1 - \frac{g}{l}\sin\theta_1\right) + \sin 2\theta_1 < 1 \right\}, \tag{21}$$

which is simply derived from (15) and (17).

4.2 Control design for the sub-FAS (20)

In this subsection, two substabilizing controllers for the sub-FAS (20) are designed and a core theorem is given. First, with the help of the FAS approach, we can design, respectively, the control inputs u_2 and u_3 as

$$u_2 = -B_1^{-1} f_1 - B_1^{-1} \boldsymbol{A}_1^{0\sim3} \theta_1^{(0\sim3)} \tag{22}$$

and

$$u_3 = -\tilde{f}_1 - \boldsymbol{A}_2^{0\sim1} \theta_3^{(0\sim1)} \tag{23}$$

within the feasible set $\mathbb{F}_1$, where $\boldsymbol{A}_1^{0\sim3} \in \mathbb{R}^{1\times4}$ and $\boldsymbol{A}_2^{0\sim1} \in \mathbb{R}^{1\times2}$ are two design vectors to make $\boldsymbol{\Phi}_1(\boldsymbol{A}_1^{0\sim3})$ and $\boldsymbol{\Phi}_2(\boldsymbol{A}_2^{0\sim1})$ Hurwitz stable.

To enhance readability, a block diagram of the closed-loop CIPS (5) is provided in Figure 2.

Now, we give the first theorem of this paper as follows.

Theorem 1. For the system (20), if the substabilizing controllers are designed as (22) and (23), then the resulting closed-loop system

$$\begin{bmatrix} \dot{\theta}_1^{(0\sim3)} \\ \dot{\theta}_3^{(0\sim1)} \end{bmatrix} = \begin{bmatrix} \boldsymbol{\Phi}_1(\boldsymbol{A}_1^{0\sim3}) & \boldsymbol{0}_{4\times2} \\ \boldsymbol{0}_{2\times4} & \boldsymbol{\Phi}_2(\boldsymbol{A}_2^{0\sim1}) \end{bmatrix} \begin{bmatrix} \theta_1^{(0\sim3)} \\ \theta_3^{(0\sim1)} \end{bmatrix} \tag{24}$$

is exponentially stable within the feasible set $\mathbb{F}_1$, and the corresponding RoEA is

$$\Xi_1=\left\{\left[\begin{array}{c}\theta_1^{(0\sim3)}(0)\\ \theta_3^{(0\sim1)}(0)\end{array}\right]\middle|\left|\frac{2m_1l^2}{k_1a^2}\left(\boldsymbol{E}_3^{\mathrm{T}}\mathrm{e}^{\boldsymbol{\Phi}_1 t}\theta_1^{(0\sim3)}(0)-\frac{g}{l}\sin\left(\boldsymbol{E}_1^{\mathrm{T}}\mathrm{e}^{\boldsymbol{\Phi}_1 t}\theta_1^{(0\sim3)}(0)\right)\right)+\sin\left(2\boldsymbol{E}_1^{\mathrm{T}}\mathrm{e}^{\boldsymbol{\Phi}_1 t}\theta_1^{(0\sim3)}(0)\right)\right|<1\right\} \tag{25}$$

with

$$\boldsymbol{E}_1=\left[\begin{array}{cccc}1&0&0&0\end{array}\right]^{\mathrm{T}},\boldsymbol{E}_3=\left[\begin{array}{cccc}0&0&1&0\end{array}\right]^{\mathrm{T}}.$$

Proof. Substituting (22) and (23) into (20), one has

$$\dot{\theta}_1^{(0\sim3)}=\boldsymbol{\Phi}_1(\boldsymbol{A}_1^{0\sim3})\theta_1^{(0\sim3)} \tag{26}$$

and

$$\dot{\theta}_3^{(0\sim1)}=\boldsymbol{\Phi_2}(\boldsymbol{A}_2^{0\sim1})\theta_3^{(0\sim1)}. \tag{27}$$

It is obvious from (26) and (27) that

$$\theta_1^{(0\sim3)}(t)=\mathrm{e}^{\boldsymbol{\Phi_1}t}\theta_1^{(0\sim3)}(0) \tag{28}$$

and

$$\theta_3^{(0\sim1)}(t)=\mathrm{e}^{\boldsymbol{\Phi_2}t}\theta_3^{(0\sim1)}(0), \tag{29}$$

which intuitively indicate that the system (24) is exponentially stable within the feasible set $\mathbb{F}_1$. Therefore, we have

$$\left\{\begin{array}{l}\theta_1(t)=\boldsymbol{E}_1^{\mathrm{T}}\mathrm{e}^{\boldsymbol{\Phi}_1 t}\theta_1^{(0\sim3)}(0),\\ \ddot{\theta}_1(t)=\boldsymbol{E}_3^{\mathrm{T}}\mathrm{e}^{\boldsymbol{\Phi_1}t}\theta_1^{(0\sim3)}(0).\end{array}\right. \tag{30}$$

Then, substituting (30) into (21), we obtain the RoEA (25) of the system (20). Further, according to (13) and (16), once $\theta_1^{(0\sim3)}$ converges into 0, θ_2 and $\dot{\theta}_2$ will also converge into 0, which indicates that the closed-loop system (5) is asymptotically stable within the feasible set $\mathbb{F}_1$.

It should be noted from (25) that the RoEA Ξ_1 imposes the following constraint only on $\theta_1^{(0\sim3)}(0)$:

$$\tilde{\Xi}_1=\left\{\theta_1^{(0\sim3)}(0)\middle|\left|\frac{2m_1l^2}{k_1a^2}\left(\boldsymbol{E}_3^{\mathrm{T}}\mathrm{e}^{\boldsymbol{\Phi}_1 t}\theta_1^{(0\sim3)}(0)-\frac{g}{l}\sin\left(\boldsymbol{E}_1^{\mathrm{T}}\mathrm{e}^{\boldsymbol{\Phi}_1 t}\theta_1^{(0\sim3)}(0)\right)\right)+\sin\left(2\boldsymbol{E}_1^{\mathrm{T}}\mathrm{e}^{\boldsymbol{\Phi}_1 t}\theta_1^{(0\sim3)}(0)\right)\right|<1\right\}. \tag{31}$$

Now, we present the following proposition to show some characteristics of the set $\tilde{\Xi}_1$.

Proposition 1. The set $\tilde{\Xi}_1$ is symmetric with respect to the origin. Furthermore, it is also bounded when the eigenvalues of the closed-loop system (26) are distinct.

Proof. In order to prove the symmetry, from (31), we define the function

$$\Gamma(X)=\frac{2m_1l^2}{k_1a^2}\left(\boldsymbol{E}_3^{\mathrm{T}}\mathrm{e}^{\boldsymbol{\Phi}_1 t}X-\frac{g}{l}\sin\left(\boldsymbol{E}_1^{\mathrm{T}}\mathrm{e}^{\boldsymbol{\Phi}_1 t}X\right)\right)+\sin\left(2\boldsymbol{E}_1^{\mathrm{T}}\mathrm{e}^{\boldsymbol{\Phi}_1 t}X\right).$$

Then, substituting the variable X in the function Γ by $-X$ yields

$$\begin{aligned}\Gamma(-X)&=\frac{2m_1l^2}{k_1a^2}\left(-\boldsymbol{E}_3^{\mathrm{T}}\mathrm{e}^{\boldsymbol{\Phi}_1 t}X-\frac{g}{l}\sin\left(-\boldsymbol{E}_1^{\mathrm{T}}\mathrm{e}^{\boldsymbol{\Phi}_1 t}X\right)\right)+\sin\left(-2\boldsymbol{E}_1^{\mathrm{T}}\mathrm{e}^{\boldsymbol{\Phi}_1 t}X\right)\\&=-\frac{2m_1l^2}{k_1a^2}\left(\boldsymbol{E}_3^{\mathrm{T}}\mathrm{e}^{\boldsymbol{\Phi}_1 t}X-\frac{g}{l}\sin\left(\boldsymbol{E}_1^{\mathrm{T}}\mathrm{e}^{\boldsymbol{\Phi}_1 t}X\right)\right)-\sin\left(2\boldsymbol{E}_1^{\mathrm{T}}\mathrm{e}^{\boldsymbol{\Phi}_1 t}X\right)\\&=-\Gamma(X),\end{aligned}$$

which directly indicates that the set $\tilde{\Xi}_1$ is symmetric with respect to the origin.

For the proof of the boundedness, according to the closed-loop system (26), it is obvious that

$$\theta_1^{(4)}=-a_0\theta_1-a_1\dot{\theta}_1-a_2\ddot{\theta}_1-a_3\theta_1^{(3)}. \tag{32}$$

Then, one has

$$\lambda_i^4+a_3\lambda_i^3+a_2\lambda_i^2+a_1\lambda_i+a_0=0, \tag{33}$$

where λ_i, $i=1,2,3,4$ are the corresponding distinct eigenvalues of the matrix $\boldsymbol{\Phi}_1\left(\boldsymbol{A}_1^{0\sim 3}\right)$. Then, we have

$$\theta_1(t)=\left[\begin{array}{cccc}\mathrm{e}^{\lambda_1 t} & \mathrm{e}^{\lambda_2 t} & \mathrm{e}^{\lambda_3 t} & \mathrm{e}^{\lambda_4 t}\end{array}\right]\left[\begin{array}{c}v_1\\ v_2\\ v_3\\ v_4\end{array}\right], \tag{34}$$

where v_i, $i=1,2,3,4$ are a set of proper constants dependent on $\theta_1^{(0\sim 3)}(0)$. Therein, $v_i\in\mathbb{R}$ if $\lambda_i\in\mathbb{R}$, and $v_i=\bar{v}_j$ if $\lambda_i=\bar{\lambda}_j$ for $i,j=1,2,3,4$.

Thus, from (34), there are

$$\left[\begin{array}{c}\theta_1(0)\\ \dot{\theta}_1(0)\\ \ddot{\theta}_1(0)\\ \theta_1^{(3)}(0)\end{array}\right]=\left[\begin{array}{cccc}1 & 1 & 1 & 1\\ \lambda_1 & \lambda_2 & \lambda_3 & \lambda_4\\ \lambda_1^2 & \lambda_2^2 & \lambda_3^2 & \lambda_4^2\\ \lambda_1^3 & \lambda_2^3 & \lambda_3^3 & \lambda_4^3\end{array}\right]\left[\begin{array}{c}v_1\\ v_2\\ v_3\\ v_4\end{array}\right] \tag{35}$$

and

$$\ddot{\theta}_1(t)=\left[\begin{array}{cccc}\lambda_1^2\mathrm{e}^{\lambda_1 t} & \lambda_2^2\mathrm{e}^{\lambda_2 t} & \lambda_3^2\mathrm{e}^{\lambda_3 t} & \lambda_4^2\mathrm{e}^{\lambda_4 t}\end{array}\right]\left[\begin{array}{c}v_1\\ v_2\\ v_3\\ v_4\end{array}\right]. \tag{36}$$

According to the feasible set (21), it can be obtained that

$$-\frac{k_1a^2}{m_1l^2}-\frac{g}{l}\leqslant\ddot{\theta}_1(t)\leqslant\frac{k_1a^2}{m_1l^2}+\frac{g}{l}. \tag{37}$$

Choosing $t=0,1,2,3$, yields

$$\left[\begin{array}{cccc}\ddot{\theta}_1(0) & \ddot{\theta}_1(1) & \ddot{\theta}_1(2) & \ddot{\theta}_1(3)\end{array}\right]\left[\begin{array}{c}\ddot{\theta}_1(0)\\ \ddot{\theta}_1(1)\\ \ddot{\theta}_1(2)\\ \ddot{\theta}_1(3)\end{array}\right]\leqslant 4\left(\frac{k_1a^2}{m_1l^2}+\frac{g}{l}\right)^2. \tag{38}$$

From (35) and (36), there is

$$\begin{aligned}\left[\begin{array}{c}\ddot{\theta}_1(0)\\ \ddot{\theta}_1(1)\\ \ddot{\theta}_1(2)\\ \ddot{\theta}_1(3)\end{array}\right]&=\left[\begin{array}{cccc}1 & 1 & 1 & 1\\ \mathrm{e}^{\lambda_1} & \mathrm{e}^{\lambda_2} & \mathrm{e}^{\lambda_3} & \mathrm{e}^{\lambda_4}\\ \mathrm{e}^{2\lambda_1} & \mathrm{e}^{2\lambda_2} & \mathrm{e}^{2\lambda_3} & \mathrm{e}^{2\lambda_4}\\ \mathrm{e}^{3\lambda_1} & \mathrm{e}^{3\lambda_2} & \mathrm{e}^{3\lambda_3} & \mathrm{e}^{3\lambda_4}\end{array}\right]\left[\begin{array}{cccc}\lambda_1^2 & & & \\ & \lambda_2^2 & & \\ & & \lambda_3^2 & \\ & & & \lambda_4^2\end{array}\right]\left[\begin{array}{cccc}1 & 1 & 1 & 1\\ \lambda_1 & \lambda_2 & \lambda_3 & \lambda_4\\ \lambda_1^2 & \lambda_2^2 & \lambda_3^2 & \lambda_4^2\\ \lambda_1^3 & \lambda_2^3 & \lambda_3^3 & \lambda_4^3\end{array}\right]^{-1}\left[\begin{array}{c}\theta_1(0)\\ \dot{\theta}_1(0)\\ \ddot{\theta}_1(0)\\ \theta_1^{(3)}(0)\end{array}\right]\\ &\triangleq\boldsymbol{Q}\theta_1^{(0\sim 3)}(0).\end{aligned} \tag{39}$$

Then, according to (38) and (39), one has

$$\lambda_{\min}\left(\boldsymbol{Q}^{\mathrm{T}}\boldsymbol{Q}\right)\left\|\theta_1^{(0\sim 3)}(0)\right\|^2\leqslant\left(\theta_1^{(0\sim 3)}(0)\right)^{\mathrm{T}}\boldsymbol{Q}^{\mathrm{T}}\boldsymbol{Q}\theta_1^{(0\sim 3)}(0)\leqslant 4\left(\frac{k_1a^2}{m_1l^2}+\frac{g}{l}\right)^2, \tag{40}$$

where $\lambda_{\min}\left(\boldsymbol{Q}^{\mathrm{T}}\boldsymbol{Q}\right)$ is the smallest eigenvalue of the square matrix $\boldsymbol{Q}^{\mathrm{T}}\boldsymbol{Q}$. Thus, we have

$$\left\|\theta_1^{(0\sim 3)}(0)\right\|\leqslant\frac{2\left(\frac{k_1a^2}{m_1l^2}+\frac{g}{l}\right)}{\sqrt{\lambda_{\min}\left(\boldsymbol{Q}^{\mathrm{T}}\boldsymbol{Q}\right)}}, \tag{41}$$

which proves the boundedness of the set $\tilde{\Xi}_1$.

Next, to give an additional research result of this paper, we briefly analyze a symmetrical scenario regarding the above control problem, in which the control input u_3 fails entirely. Therefore, the original system (4) is changed into

$$S_\delta : \begin{cases} S_1 : \ddot{\theta}_1 = \frac{g}{l}\sin\theta_1 + \frac{k_1 a^2}{m_1 l^2}\left(\sin\theta_2\cos\theta_2 - \sin\theta_1\cos\theta_1\right) + u_1, \\ S_2 : \ddot{\theta}_2 = \frac{g}{l}\sin\theta_2 + \frac{k_1 a^2}{m_2 l^2}\left(\sin\theta_1\cos\theta_1 - \sin\theta_2\cos\theta_2\right) + \frac{k_2 a^2}{m_2 l^2}\left(\sin\theta_3\cos\theta_3 - \sin\theta_2\cos\theta_2\right) + u_2, \\ S_3 : \ddot{\theta}_3 = \frac{g}{l}\sin\theta_3 + \frac{k_2 a^2}{m_3 l^2}\left(\sin\theta_2\cos\theta_2 - \sin\theta_3\cos\theta_3\right). \end{cases} \tag{42}$$

Then, through a set of differentiation and variable substitution analogous to the aforementioned process, the system (42) is transformed into the corresponding sub-FAS model:

$$\begin{bmatrix} \ddot{\theta}_1 \\ \theta_3^{(4)} \end{bmatrix} = \begin{bmatrix} \tilde{f}_1^* \\ f_1^* \end{bmatrix} + \begin{bmatrix} 1 & 0 \\ 0 & B_1^* \end{bmatrix} \begin{bmatrix} u_1 \\ u_2 \end{bmatrix} \tag{43}$$

with the following feasible set:

$$\mathbb{F}_1^* = \left\{ \begin{bmatrix} \theta_1^{(0\sim1)} \\ \theta_3^{(0\sim3)} \end{bmatrix} \middle| -1 < \frac{2m_3 l^2}{k_2 a^2}\left(\ddot{\theta}_3 - \frac{g}{l}\sin\theta_3\right) + \sin 2\theta_3 < 1 \right\}, \tag{44}$$

where $\tilde{f}_1^*$, f_1^* and B_1^* are three appropriate functions computable similarly to the process in Subsection 4.1.

Then, based on the FAS approach, in the feasible set $\mathbb{F}_1^*$, design the controllers u_1 and u_2 as

$$u_1 = -\tilde{f}_1^* - \boldsymbol{A}_1^{*0\sim1}\theta_1^{(0\sim1)} \tag{45}$$

and

$$u_2 = -B_1^{*-1} f_1^* - B_1^{*-1}\boldsymbol{A}_2^{*0\sim3}\theta_3^{(0\sim3)} \tag{46}$$

with $\boldsymbol{A}_1^{*0\sim1} \in \mathbb{R}^{1\times2}$ and $\boldsymbol{A}_2^{*0\sim3} \in \mathbb{R}^{1\times4}$ being two design vectors to ensure that $\boldsymbol{\Phi}_1\left(\boldsymbol{A}_1^{*0\sim1}\right)$ and $\boldsymbol{\Phi_2}\left(\boldsymbol{A}_2^{*0\sim3}\right)$ are Hurwitz.

Now, we obtain the following theorem.

Theorem 2. For the system (43), if the substabilizing controllers are designed as (45) and (46), then the resulting closed-loop system

$$\begin{bmatrix} \dot{\theta}_1^{(0\sim1)} \\ \dot{\theta}_3^{(0\sim3)} \end{bmatrix} = \begin{bmatrix} \boldsymbol{\Phi}_1(\boldsymbol{A}_1^{*0\sim1}) & \boldsymbol{0}_{2\times4} \\ \boldsymbol{0}_{4\times2} & \boldsymbol{\Phi}_2(\boldsymbol{A}_2^{*0\sim3}) \end{bmatrix} \begin{bmatrix} \theta_1^{(0\sim1)} \\ \theta_3^{(0\sim3)} \end{bmatrix} \tag{47}$$

is exponentially stable within the feasible set $\mathbb{F}_1^*$, and the corresponding RoEA is

$$\Xi_1^* = \left\{ \begin{bmatrix} \theta_1^{(0\sim1)}(0) \\ \theta_3^{(0\sim3)}(0) \end{bmatrix} \middle| \left| \frac{2m_3 l^2}{k_2 a^2}\left(\boldsymbol{E}_3^{\mathrm{T}}\mathrm{e}^{\boldsymbol{\Phi}_2 t}\theta_3^{(0\sim3)}(0) - \frac{g}{l}\sin\left(\boldsymbol{E}_1^{\mathrm{T}}\mathrm{e}^{\boldsymbol{\Phi}_2 t}\theta_3^{(0\sim3)}(0)\right)\right) + \sin\left(2\boldsymbol{E}_1^{\mathrm{T}}\mathrm{e}^{\boldsymbol{\Phi}_2 t}\theta_3^{(0\sim3)}(0)\right) \right| < 1 \right\}. \tag{48}$$

The proof of Theorem 2 parallels that of Theorem 1 and is omitted for brevity.

5 Substabilization for the CIPS (6)

Similar to Section 4, in this section, we convert the system (6) into its corresponding sub-FAS model. Then, for the obtained sub-FAS, the substabilizing controllers are designed, and the corresponding RoEA is given.

5.1 Sub-FAS model of the CIPS (6)

First, it is obvious from the subsystem S_2 of the system (6) that

$$\theta_2^{(3)} = \frac{g}{l}\dot{\theta}_2\cos\theta_2 + \frac{k_1 a^2}{m_2 l^2}\dot{\theta}_1\cos2\theta_1 - \frac{k_1 a^2}{m_2 l^2}\dot{\theta}_2\cos2\theta_2 + \frac{k_2 a^2}{m_2 l^2}\dot{\theta}_3\cos2\theta_3 - \frac{k_2 a^2}{m_2 l^2}\dot{\theta}_2\cos2\theta_2. \tag{49}$$

Then, taking the derivatives for two sides of (49), it can be obtained that

$$\theta_2^{(4)} = \frac{g}{l}\left(\ddot{\theta}_2\cos\theta_2 - \dot{\theta}_2^2\sin\theta_2\right) + \frac{k_1 a^2}{m_2 l^2}\left(\ddot{\theta}_1\cos2\theta_1 - 2\dot{\theta}_1^2\sin2\theta_1\right) - \frac{k_1 a^2}{m_2 l^2}\left(\ddot{\theta}_2\cos2\theta_2 - 2\dot{\theta}_2^2\sin2\theta_2\right)$$

$$+\frac{k_2a^2}{m_2l^2}\left(\ddot{\theta}_3\cos 2\theta_3-2\dot{\theta}_3^2\sin 2\theta_3\right)-\frac{k_2a^2}{m_2l^2}\left(\ddot{\theta}_2\cos 2\theta_2-2\dot{\theta}_2^2\sin 2\theta_2\right). \tag{50}$$

Now, we substitute the subsystems S_1 and S_3 of the system (6) into (50), which obtains

$$\begin{aligned}\theta_2^{(4)}=&\frac{g}{l}\left(\ddot{\theta}_2\cos\theta_2-\dot{\theta}_2^2\sin\theta_2\right)+\frac{k_1a^2}{m_2l^2}\left(\left(\frac{g}{l}\sin\theta_1+\frac{k_1a^2}{2m_1l^2}\left(\sin 2\theta_2-\sin 2\theta_1\right)+u_1\right)\cos 2\theta_1-2\dot{\theta}_1^2\sin 2\theta_1\right)\\&-\frac{k_1a^2}{m_2l^2}\left(\ddot{\theta}_2\cos 2\theta_2-2\dot{\theta}_2^2\sin 2\theta_2\right)\\&+\frac{k_2a^2}{m_2l^2}\left(\left(\frac{g}{l}\sin\theta_3+\frac{k_2a^2}{2m_3l^2}\left(\sin 2\theta_2-\sin 2\theta_3\right)+u_3\right)\cos 2\theta_3-2\dot{\theta}_3^2\sin 2\theta_3\right)\\&-\frac{k_2a^2}{m_2l^2}\left(\ddot{\theta}_2\cos 2\theta_2-2\dot{\theta}_2^2\sin 2\theta_2\right).\end{aligned} \tag{51}$$

From the subsystem S_2 of the system (6), there is

$$\sin 2\theta_3=\frac{2m_2l^2}{k_2a^2}\left(\ddot{\theta}_2-\frac{g}{l}\sin\theta_2-\frac{k_1a^2}{2m_2l^2}\left(\sin 2\theta_1-\sin 2\theta_2\right)+\frac{k_2a^2}{2m_2l^2}\sin 2\theta_2\right), \tag{52}$$

namely,

$$\begin{aligned}\theta_3=&\frac{1}{2}\arcsin\left(\frac{2m_2l^2}{k_2a^2}\ddot{\theta}_2-\frac{2m_2gl}{k_2a^2}\sin\theta_2-\frac{k_1}{k_2}\left(\sin 2\theta_1-\sin 2\theta_2\right)+\sin 2\theta_2\right)\\=&\Psi_1\left(\theta_1,\theta_2,\ddot{\theta}_2\right)\end{aligned} \tag{53}$$

with the following constraint:

$$-1\leqslant\Psi_2\left(\theta_1,\theta_2,\ddot{\theta}_2\right)\leqslant 1, \tag{54}$$

where

$$\Psi_2\left(\theta_1,\theta_2,\ddot{\theta}_2\right)=\frac{2m_2l^2}{k_2a^2}\ddot{\theta}_2-\frac{2m_2gl}{k_2a^2}\sin\theta_2-\frac{k_1}{k_2}\left(\sin 2\theta_1-\sin 2\theta_2\right)+\sin 2\theta_2.$$

Further, it can be known from (53) that $\dot{\theta}_3$ satisfies

$$\begin{aligned}\dot{\theta}_3=&\frac{\left(\frac{2m_2l^2}{k_2a^2}\ddot{\theta}_2-\frac{2m_2gl}{k_2a^2}\sin\theta_2-\frac{k_1}{k_2}\left(\sin 2\theta_1-\sin 2\theta_2\right)+\sin 2\theta_2\right)'}{2\sqrt{1-\Psi_2^2}}\\=&\frac{1}{2\sqrt{1-\Psi_2^2}}\left(\frac{2m_2l^2}{k_2a^2}\theta_2^{(3)}-\frac{2m_2gl}{k_2a^2}\dot{\theta}_2\cos\theta_2-\frac{2k_1}{k_2}\left(\dot{\theta}_1\cos 2\theta_1-\dot{\theta}_2\cos 2\theta_2\right)+2\dot{\theta}_2\cos 2\theta_2\right)\\=&\Psi_3\left(\theta_1^{(0\sim 1)},\theta_2^{(0\sim 3)}\right),\end{aligned} \tag{55}$$

where

$$\Psi_3\left(\theta_1^{(0\sim 1)},\theta_2^{(0\sim 3)}\right)=\frac{1}{2\sqrt{1-\Psi_2^2}}\left(\frac{2m_2l^2}{k_2a^2}\theta_2^{(3)}-\frac{2m_2gl}{k_2a^2}\dot{\theta}_2\cos\theta_2-\frac{2k_1}{k_2}\left(\dot{\theta}_1\cos 2\theta_1-\dot{\theta}_2\cos 2\theta_2\right)+2\dot{\theta}_2\cos 2\theta_2\right),$$

which requires

$$-1<\Psi_2\left(\theta_1,\theta_2,\ddot{\theta}_2\right)<1. \tag{56}$$

Then, according to (53) and (55), we can replace θ_3 and $\dot{\theta}_3$ by $\Psi_1\left(\theta_1,\theta_2,\ddot{\theta}_2\right)$ and $\Psi_3\left(\theta_1^{(0\sim 1)},\theta_2^{(0\sim 3)}\right)$, which makes (51) changed into

$$\begin{aligned}\theta_2^{(4)}=&\frac{g}{l}\left(\ddot{\theta}_2\cos\theta_2-\dot{\theta}_2^2\sin\theta_2\right)+\frac{k_1a^2}{m_2l^2}\left(\left(\frac{g}{l}\sin\theta_1+\frac{k_1a^2}{2m_1l^2}\left(\sin 2\theta_2-\sin 2\theta_1\right)+u_1\right)\cos 2\theta_1-2\dot{\theta}_1^2\sin 2\theta_1\right)\\&-\frac{k_1a^2}{m_2l^2}\left(\ddot{\theta}_2\cos 2\theta_2-2\dot{\theta}_2^2\sin 2\theta_2\right)\end{aligned}$$

$$
\begin{aligned}
&+\frac{k_2a^2}{m_2l^2}\left(\left(\frac{g}{l}\sin\Psi_1+\frac{k_2a^2}{2m_3l^2}\left(\sin 2\theta_2-\sin 2\Psi_1\right)+u_3\right)\cos 2\Psi_1-2\Psi_3^2\sin 2\Psi_1\right)\\
&-\frac{k_2a^2}{m_2l^2}\left(\ddot{\theta}_2\cos 2\theta_2-2\dot{\theta}_2^2\sin 2\theta_2\right)\\
=&f_2+u_1\frac{k_1a^2}{m_2l^2}\cos 2\theta_1+u_3\frac{k_2a^2}{m_2l^2}\cos 2\Psi_1
\end{aligned}\tag{57}
$$

with

$$
\begin{aligned}
f_2\left(\theta_1^{(0\sim1)},\theta_2^{(0\sim3)}\right)=&\frac{g}{l}\ddot{\theta}_2\cos\theta_2-\frac{g}{l}\dot{\theta}_2^2\sin\theta_2+\frac{k_1a^2g}{m_2l^3}\sin\theta_1\cos 2\theta_1\\
&+\frac{k_1a^2}{m_2l^2}\left(\sin 2\theta_2-\sin 2\theta_1\right)\left(\frac{k_1a^2}{2m_1l^2}\cos 2\theta_1+2\dot{\theta}_1^2\right)-\frac{k_1a^2}{m_2l^2}\ddot{\theta}_2\cos 2\theta_2\\
&+\frac{k_2a^2}{m_2l^2}\left(\frac{g}{l}\sin\Psi_1\cos 2\Psi_1+\frac{k_2a^2}{2m_3l^2}\sin 2\theta_2\cos 2\Psi_1-\frac{k_2a^2}{2m_3l^2}\sin 2\Psi_1\cos 2\Psi_1\right.\\
&\left.-2\Psi_3^2\sin 2\Psi_1-\ddot{\theta}_2\cos 2\theta_2+2\dot{\theta}_2^2\sin 2\theta_2\right).
\end{aligned}\tag{58}
$$

Therefore, we can obtain the corresponding sub-FAS model of the system (6) as follows:

$$
\begin{bmatrix}\ddot{\theta}_1\\ \theta_2^{(4)}\end{bmatrix}=\begin{bmatrix}\tilde{f}_2\\ f_2\end{bmatrix}+\begin{bmatrix}1 & 0\\ \frac{k_1a^2}{m_2l^2}\cos 2\theta_1 & \frac{k_2a^2}{m_2l^2}\cos 2\Psi_1\end{bmatrix}\begin{bmatrix}u_1\\ u_3\end{bmatrix}\tag{59}
$$

with the feasible set

$$
\mathbb{F}_2=\left\{\begin{bmatrix}\theta_1^{(0\sim1)}\\ \theta_2^{(0\sim3)}\end{bmatrix}\middle|-1<\frac{2m_2l^2}{k_2a^2}\ddot{\theta}_2-\frac{2m_2gl}{k_2a^2}\sin\theta_2-\frac{k_1}{k_2}\left(\sin 2\theta_1-\sin 2\theta_2\right)+\sin 2\theta_2<1\right\},\tag{60}
$$

where

$$
\tilde{f}_2=\frac{g}{l}\sin\theta_1+\frac{k_1a^2}{m_1l^2}\left(\sin\theta_2\cos\theta_2-\sin\theta_1\cos\theta_1\right).
$$

5.2 Control design for the sub-FAS (59)

Now, we start to design the substabilizing controllers for the sub-FAS (59). In the feasible set $\mathbb{F}_2$, two controllers u_1 and u_3 are, respectively, designed as

$$
u_1=-\tilde{f}_2-\tilde{\boldsymbol{A}}_1^{0\sim1}\theta_1^{(0\sim1)}\tag{61}
$$

and

$$
\begin{aligned}
u_3=&-\frac{m_2l^2}{k_2a^2\cos 2\Psi_1}\left(f_2+\frac{k_1a^2\cos 2\theta_1}{m_2l^2}u_1+\tilde{\boldsymbol{A}}_2^{0\sim3}\theta_2^{(0\sim3)}\right)\\
=&-\frac{m_2l^2}{k_2a^2\cos 2\Psi_1}\left(f_2-\frac{k_1a^2\cos 2\theta_1}{m_2l^2}\left(\tilde{f}_2+\tilde{\boldsymbol{A}}_1^{0\sim1}\theta_1^{(0\sim1)}\right)+\tilde{\boldsymbol{A}}_2^{0\sim3}\theta_2^{(0\sim3)}\right),
\end{aligned}\tag{62}
$$

where $\tilde{\boldsymbol{A}}_1^{0\sim1}\in\mathbb{R}^{1\times2}$ and $\tilde{\boldsymbol{A}}_2^{0\sim3}\in\mathbb{R}^{1\times4}$ are also two design vectors to make $\boldsymbol{\Phi}_1(\tilde{\boldsymbol{A}}_1^{0\sim1})$ and $\boldsymbol{\Phi}_2(\tilde{\boldsymbol{A}}_2^{0\sim3})$ Hurwitz.

In order to show the third theorem of this paper, we first define the following three vectors:

$$
\boldsymbol{E}_{11}=\begin{bmatrix}1&0\end{bmatrix}^{\mathrm{T}},\ \boldsymbol{E}_{21}=\begin{bmatrix}1&0&0&0\end{bmatrix}^{\mathrm{T}},\ \boldsymbol{E}_{23}=\begin{bmatrix}0&0&1&0\end{bmatrix}^{\mathrm{T}}.\tag{63}
$$

Correspondingly, the block diagram about the closed-loop system (6) is shown in Figure 3.

Then, the third theorem of this paper is given as follows.

Theorem 3. For the sub-FAS (59), if the substabilizing controllers are designed as (61) and (62), then the resulting closed-loop system

$$
\begin{bmatrix}\dot{\theta}_1^{(0\sim1)}\\ \dot{\theta}_2^{(0\sim3)}\end{bmatrix}=\begin{bmatrix}\boldsymbol{\Phi}_1(\tilde{\boldsymbol{A}}_1^{0\sim1}) & \boldsymbol{0}_{2\times4}\\ \boldsymbol{0}_{4\times2} & \boldsymbol{\Phi}_2(\tilde{\boldsymbol{A}}_2^{0\sim3})\end{bmatrix}\begin{bmatrix}\theta_1^{(0\sim1)}\\ \theta_2^{(0\sim3)}\end{bmatrix}\tag{64}
$$

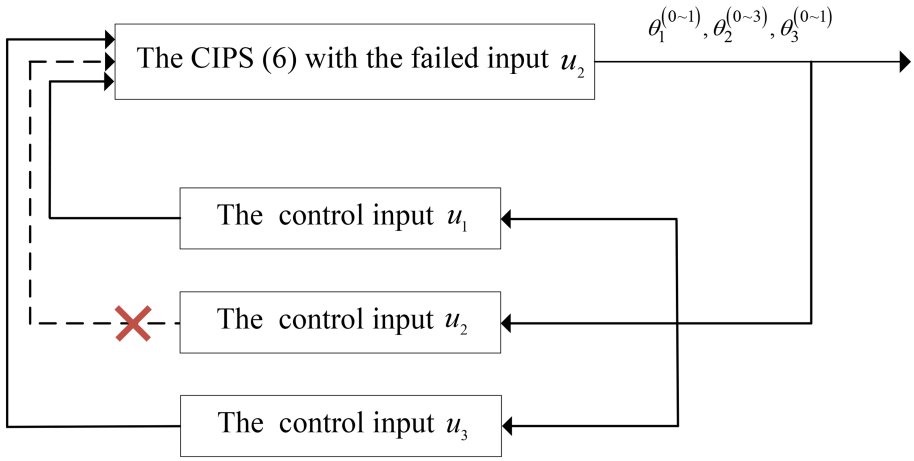

Figure 3 (Color online) The block diagram of the closed-loop system (6).

is exponentially stable within the feasible set $\mathbb{F}_2$, and the corresponding RoEA is

$$\Xi_2 = \left\{ \begin{bmatrix} \theta_1^{(0\sim1)}(0) \\ \theta_2^{(0\sim3)}(0) \end{bmatrix} \middle| \begin{array}{l} \left| \frac{2m_2l^2}{k_2a^2} \boldsymbol{E}_{23}^{\mathrm{T}} \mathrm{e}^{\boldsymbol{\Phi}_2 t} \theta_2^{(0\sim3)}(0) - \frac{k_1}{k_2} \left(\sin\left(2\boldsymbol{E}_{11}^{\mathrm{T}} \mathrm{e}^{\boldsymbol{\Phi}_1 t} \theta_1^{(0\sim1)}(0) \right) - \sin\left(2\boldsymbol{E}_{21}^{\mathrm{T}} \mathrm{e}^{\boldsymbol{\Phi}_2 t} \theta_2^{(0\sim3)}(0) \right) \right) \right. \\ \left. -\frac{2m_2gl}{k_2a^2} \sin\left(\boldsymbol{E}_{21}^{\mathrm{T}} \mathrm{e}^{\boldsymbol{\Phi}_2 t} \theta_2^{(0\sim3)}(0) \right) + \sin\left(2\boldsymbol{E}_{21}^{\mathrm{T}} \mathrm{e}^{\boldsymbol{\Phi}_2 t} \theta_2^{(0\sim3)}(0) \right) \right| < 1 \end{array} \right\}. \tag{65}$$

Proof. We substitute (61) and (62) into (59), which yields

$$\dot{\theta}_1^{(0\sim1)} = \boldsymbol{\Phi}_1(\tilde{\boldsymbol{A}}_1^{0\sim1})\theta_1^{(0\sim1)} \tag{66}$$

and

$$\dot{\theta}_2^{(0\sim3)} = \boldsymbol{\Phi}_2(\tilde{\boldsymbol{A}}_2^{0\sim3})\theta_2^{(0\sim3)}. \tag{67}$$

Therefore, there are

$$\theta_1^{(0\sim1)}(t) = \mathrm{e}^{\boldsymbol{\Phi}_1 t}\theta_1^{(0\sim1)}(0) \tag{68}$$

and

$$\theta_2^{(0\sim3)}(t) = \mathrm{e}^{\boldsymbol{\Phi}_2 t}\theta_2^{(0\sim3)}(0), \tag{69}$$

which illustrate that the closed-loop system (64) is exponentially stable within the feasible set $\mathbb{F}_2$.

Then, from (68) and (69), we have

$$\begin{cases} \theta_1(t) = \boldsymbol{E}_{11}^{\mathrm{T}} \mathrm{e}^{\boldsymbol{\Phi}_1 t} \theta_1^{(0\sim1)}(0), \\ \theta_2(t) = \boldsymbol{E}_{21}^{\mathrm{T}} \mathrm{e}^{\boldsymbol{\Phi}_2 t} \theta_2^{(0\sim3)}(0), \\ \ddot{\theta}_2(t) = \boldsymbol{E}_{23}^{\mathrm{T}} \mathrm{e}^{\boldsymbol{\Phi}_2 t} \theta_2^{(0\sim3)}(0). \end{cases} \tag{70}$$

Substituting (70) into the feasible set (60), one has the corresponding RoEA (65). Furthermore, from (53) and (55), $\theta_3^{(0\sim1)}$ will converge into 0 when $\theta_1^{(0\sim1)}$ and $\theta_2^{(0\sim3)}$ converge into 0. Therefore, the closed-loop CIPS (6) is asymptotically stable.

6 Simulation research

In this section, the simulation research for the CIPSs (5) and (6) is presented to demonstrate the effectiveness of the proposed method.

First, for system (5), these physical parameters g, l, k_1, k_2, m_1, m_2, m_3, and a are considered $g = 9.8$ (m/s^2), $l = 0.6$ (m), $k_1 = k_2 = 1.8$ (N/m), $m_1 = m_2 = m_3 = 0.4$ (kg), and $a = 0.3$ (m), respectively. According to Theorem 1, two substabilizing controllers u_2 and u_3 can be designed with the design vectors $\boldsymbol{A}_1^{0\sim3} = \begin{bmatrix} 192 & 232 & 98 & 17 \end{bmatrix}$ and $\boldsymbol{A}_2^{0\sim1} = \begin{bmatrix} 6 & 5 \end{bmatrix}$, respectively. It can be known from Proposition 1 that the set $\tilde{\Xi}_1$ is symmetric with respect to the origin, and is also bounded. Then, in order to show other characteristics of the set $\tilde{\Xi}_1$ under the above parameters, we provide the projections of the set $\tilde{\Xi}_1$ in the 3-D space along the $\theta_1(0)$, $\dot{\theta}_1(0)$, $\ddot{\theta}_1(0)$, and $\theta_1^{(3)}(0)$ axes in Figures

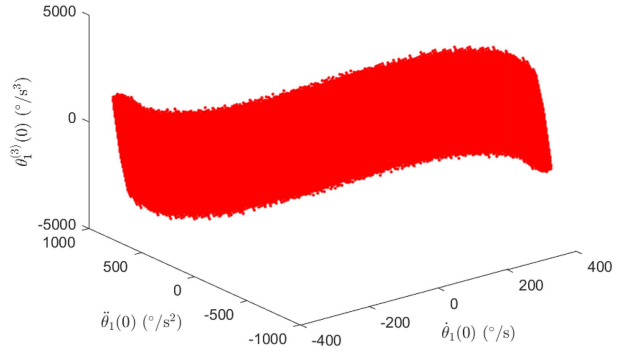

Figure 4 (Color online) The projection of $\tilde{\Xi}_1$ along the $\theta_1(0)$ axis.

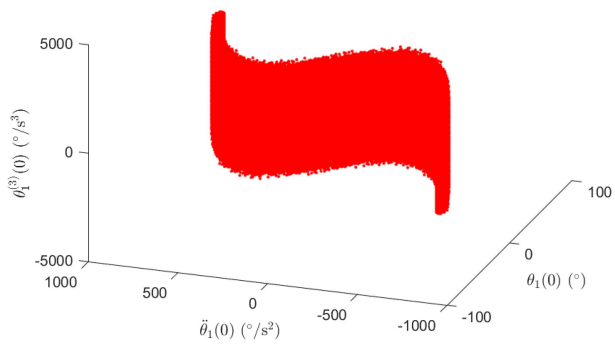

Figure 5 (Color online) The projection of $\tilde{\Xi}_1$ along the $\dot{\theta}_1(0)$ axis.

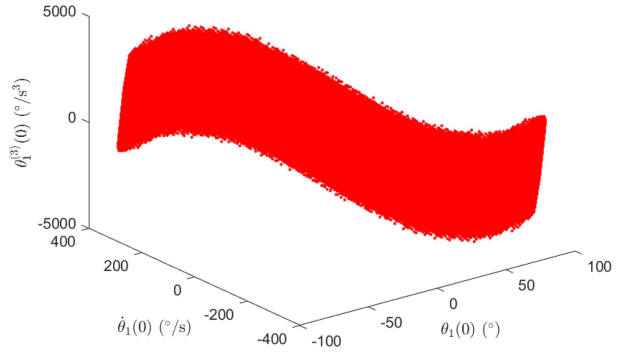

Figure 6 (Color online) The projection of $\tilde{\Xi}_1$ along the $\ddot{\theta}_1(0)$ axis.

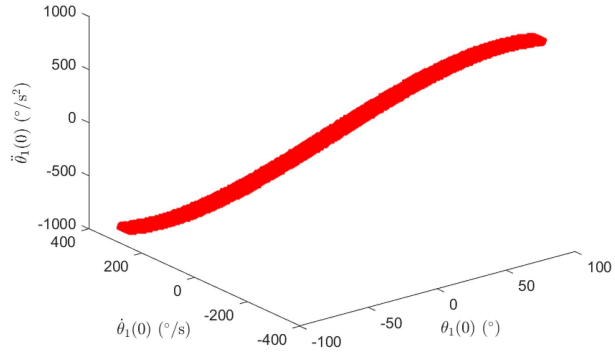

Figure 7 (Color online) The projection of $\tilde{\Xi}_1$ along the $\theta_1^{(3)}(0)$ axis.

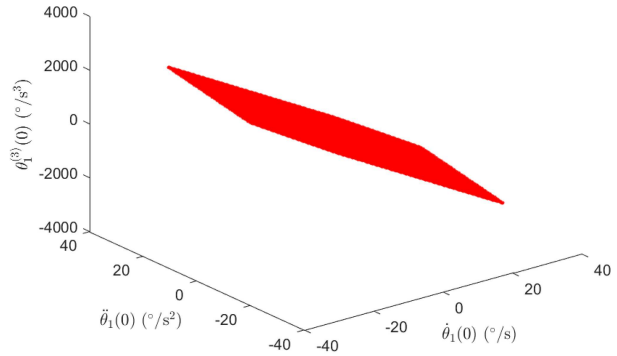

Figure 8 (Color online) The section of $\tilde{\Xi}_1$ intersected by the 4-D hyperplane $\theta_1(0) = 0$.

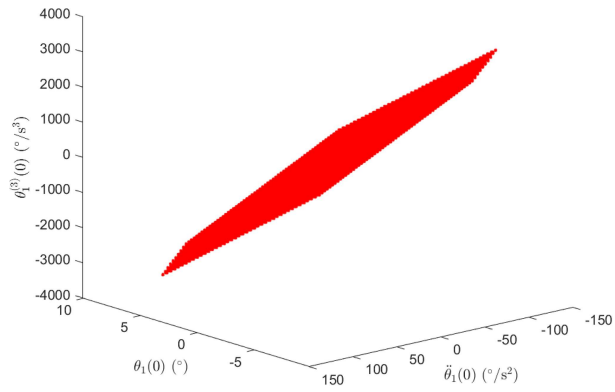

Figure 9 (Color online) The section of $\tilde{\Xi}_1$ intersected by the 4-D hyperplane $\dot{\theta}_1(0) = 0$.

4–7, respectively. The sections of the set $\tilde{\Xi}_1$ intersected by the 4-D hyperplanes $\theta_1(0) = 0$, $\dot{\theta}_1(0) = 0$, $\ddot{\theta}_1(0) = 0$, and $\theta_1^{(3)}(0) = 0$ are also shown in Figures 8–11. Furthermore, we approximately provide the inscribed hypersphere (radius ≈ 0.947) and hypercube (edge length ≈ 3.1416) of the set $\tilde{\Xi}_1$, and present the ranges of $\theta_1^{(0\sim3)}(0)$ according to (31) as follows:

$$\begin{cases} -90 < \theta_1(0) < +90, \\ -341 < \dot{\theta}_1(0) < +341, \\ -963 < \ddot{\theta}_1(0) < +963, \\ -4985 < \theta_1^{(3)}(0) < +4985. \end{cases}$$

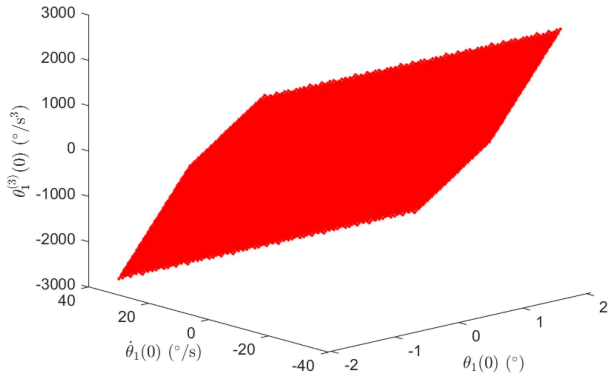

Figure 10 (Color online) The section of $\tilde{\Xi}_1$ intersected by the 4-D hyperplane $\ddot{\theta}_1(0) = 0$.

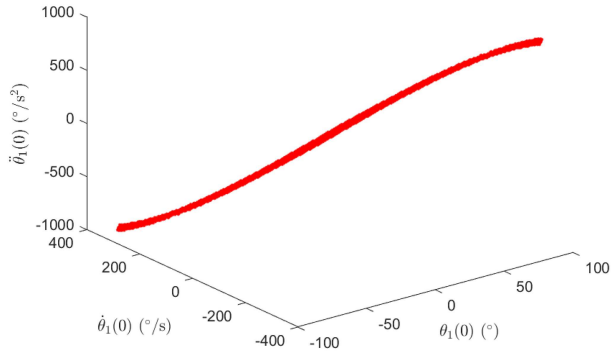

Figure 11 (Color online) The section of $\tilde{\Xi}_1$ intersected by the 4-D hyperplane $\theta_1^{(3)}(0)$.

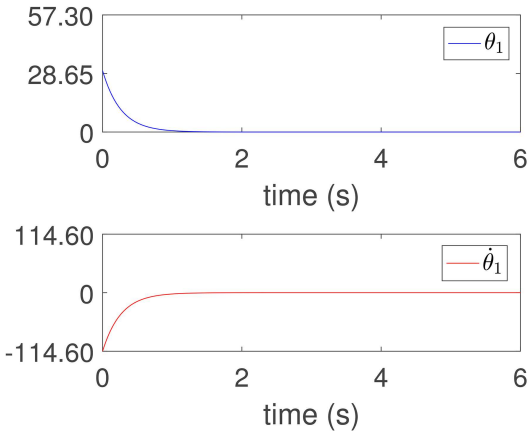

Figure 12 (Color online) The curves of θ_1 and $\dot{\theta}_1$ of the system (5).

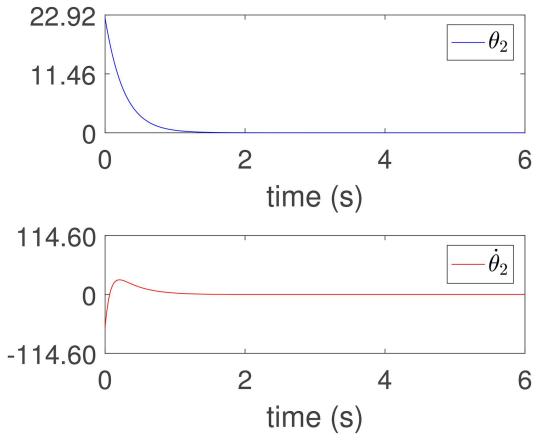

Figure 13 (Color online) The curves of θ_2 and $\dot{\theta}_2$ of the system (5).

Then, we set the system initial values as

$$\theta_1^{(0\sim3)}(0) = \begin{bmatrix} 30 & -114.6 & 435.48 & 1427.3 \end{bmatrix}^{\mathrm{T}}, \theta_3^{(0\sim1)}(0) = \begin{bmatrix} -45.84 & 45.84 \end{bmatrix}^{\mathrm{T}},$$

which are used to compute out $\theta_2^{(0\sim1)}(0) = \begin{bmatrix} 22.34 & -64.4 \end{bmatrix}^{\mathrm{T}}$. The simulation curves are shown in Figures 12–15. Therein, Figure 12 gives the curves of θ_1 and $\dot{\theta}_1$, the curves of θ_2 and $\dot{\theta}_2$ are depicted in Figure 13, and the curves of θ_3 and $\dot{\theta}_3$ and the curves of u_2 and u_3 are, respectively, given in Figures 14 and 15. It is seen from simulation results that all of the states converge into the origin, and the control inputs are within a reasonable range even if the input u_1 fails entirely, which proves the effectiveness of the proposed substabilization method.

Now, we consider the system (6). In this simulation, we keep the above physical parameters unchanged. Then, from (65), the corresponding RoEA can be obtained as follows:

$$\Xi_2 = \left\{ \begin{bmatrix} \theta_1^{(0\sim1)}(0) \\ \theta_2^{(0\sim3)}(0) \end{bmatrix} \middle| \begin{array}{l} \left| \frac{16}{9} \boldsymbol{E}_{23}^{\mathrm{T}} \mathrm{e}^{\boldsymbol{\Phi}_2 t} \theta_2^{(0\sim3)}(0) - \left(\sin\left(2\boldsymbol{E}_{11}^{\mathrm{T}} \mathrm{e}^{\boldsymbol{\Phi}_1 t} \theta_1^{(0\sim1)}(0) \right) - \sin\left(2\boldsymbol{E}_{21}^{\mathrm{T}} \mathrm{e}^{\boldsymbol{\Phi}_2 t} \theta_2^{(0\sim3)}(0) \right) \right) \right. \\ \left. -\frac{784}{27} \sin\left(\boldsymbol{E}_{21}^{\mathrm{T}} \mathrm{e}^{\boldsymbol{\Phi}_2 t} \theta_2^{(0\sim3)}(0) \right) + \sin\left(2\boldsymbol{E}_{21}^{\mathrm{T}} \mathrm{e}^{\boldsymbol{\Phi}_2 t} \theta_2^{(0\sim3)}(0) \right) \right| < 1 \end{array} \right\}. \quad (71)$$

It is easy to deduce the symmetry of the RoEA (71) with respect to the origin, so the corresponding proof is omitted here. However, due to the complexity of the RoEA Ξ_2, it is challenging to present a specific figure that captures the characteristics of the set. Nonetheless, we present the inscribed hypersphere (radius ≈ 13.48) and hypercube (edge length ≈ 15.7) of the set Ξ_2. Additionally, the approximate ranges of $\theta_1^{(0\sim1)}(0)$ and $\theta_2^{(0\sim3)}(0)$, from (71), are

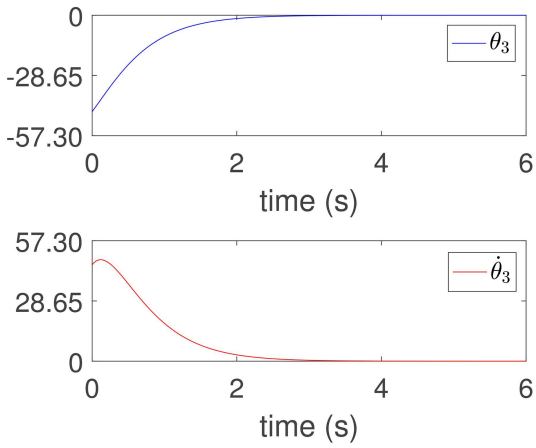

Figure 14 (Color online) The curves of θ_3 and $\dot{\theta}_3$ of the system (5).

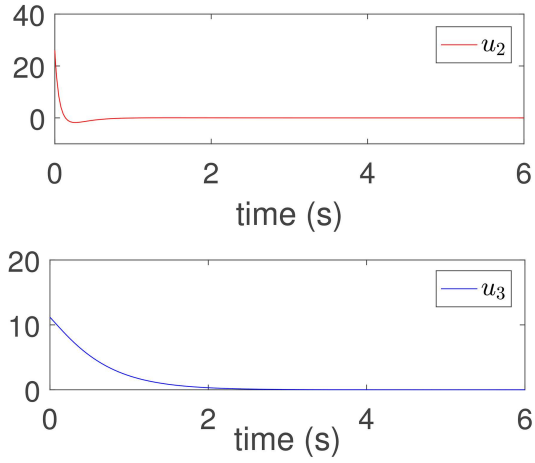

Figure 15 (Color online) The curves of u_2 and u_3 of the system (5).

as follows:

$$\begin{cases} -90 < \theta_1(0) < +90, \\ -\infty < \dot{\theta}_1(0) < +\infty, \\ -90 < \theta_2(0) < +90, \\ -343.8 < \dot{\theta}_2(0) < +343.8, \\ -974.1 < \ddot{\theta}_2(0) < +974.1, \\ -5271.6 < \theta_2^{(3)}(0) < +5271.6. \end{cases} \tag{72}$$

According to Theorem 3, the corresponding controllers u_1 and u_3 can be designed from (61) and (62) with the design vectors being $\tilde{\boldsymbol{A}}_1^{0\sim1} = \begin{bmatrix} 8 & 6 \end{bmatrix}$ and $\tilde{\boldsymbol{A}}_2^{0\sim3} = \begin{bmatrix} 144 & 180 & 80 & 15 \end{bmatrix}$. The system initial values are

$$\theta_1^{(0\sim1)}(0) = \begin{bmatrix} 45 & -229.2 \end{bmatrix}^{\mathrm{T}}, \theta_2^{(0\sim3)}(0) = \begin{bmatrix} 25.71 & -103.14 & 366.72 & -1031.4 \end{bmatrix}^{\mathrm{T}},$$

which are used to compute out $\theta_3^{(0\sim1)}(0) = \begin{bmatrix} -20.55 & 403 \end{bmatrix}^{\mathrm{T}}$. Similarly, the curves of all of the system signals are, respectively, shown in Figures 16–19. From Figures 16–19, we observe that the closed-loop system (6) is asymptotically stable, even though only two inputs are utilized, illustrating the effectiveness of the proposed method again.

Remark 1. To enhance the practicality of the proposed control method, the following guidelines are provided. First, Eqs. (25) and (65) indicate that the RoEAs of the closed-loop systems (24) and (64) are influenced by the matrices $\boldsymbol{\Phi}_1(\boldsymbol{A}_1^{0\sim3})$, $\boldsymbol{\Phi}_2(\boldsymbol{A}_2^{0\sim1})$, $\boldsymbol{\Phi}_1(\tilde{\boldsymbol{A}}_1^{0\sim1})$ and $\boldsymbol{\Phi}_2(\tilde{\boldsymbol{A}}_2^{0\sim3})$, which are directly determined by the design vectors $\boldsymbol{A}_1^{0\sim3}$, $\boldsymbol{A}_2^{0\sim1}$, $\tilde{\boldsymbol{A}}_1^{0\sim1}$ and $\tilde{\boldsymbol{A}}_2^{0\sim3}$, respectively. Consequently, when the system initial values in practical application are larger, the matrices $\boldsymbol{\Phi}_1(\boldsymbol{A}_1^{0\sim3})$, $\boldsymbol{\Phi}_2(\boldsymbol{A}_2^{0\sim1})$, $\boldsymbol{\Phi}_1(\tilde{\boldsymbol{A}}_1^{0\sim1})$ and $\boldsymbol{\Phi}_2(\tilde{\boldsymbol{A}}_2^{0\sim3})$ should be judiciously selected to ensure sufficiently large RoEAs. Furthermore, the control performance of the closed-loop systems (24) and (64) is also governed by these matrices. To achieve faster state convergence, the design vectors $\boldsymbol{A}_1^{0\sim3}$, $\boldsymbol{A}_2^{0\sim1}$, $\tilde{\boldsymbol{A}}_1^{0\sim1}$ and $\tilde{\boldsymbol{A}}_2^{0\sim3}$ should be selected such that the corresponding matrices $\boldsymbol{\Phi}_1(\boldsymbol{A}_1^{0\sim3})$, $\boldsymbol{\Phi}_2(\boldsymbol{A}_2^{0\sim1})$, $\boldsymbol{\Phi}_1(\tilde{\boldsymbol{A}}_1^{0\sim1})$ and $\boldsymbol{\Phi}_2(\tilde{\boldsymbol{A}}_2^{0\sim3})$ possess the eigenvalues with smaller real parts. Naturally, such design vectors often enlarge the control inputs, elevating energy consumption. Moreover, when additional performance requirements are imposed on the control systems, the design vectors $\boldsymbol{A}_1^{0\sim3}$, $\boldsymbol{A}_2^{0\sim1}$, $\tilde{\boldsymbol{A}}_1^{0\sim1}$ and $\tilde{\boldsymbol{A}}_2^{0\sim3}$ must be adjusted to configure the specific eigenstructure. In summary, practical applicability demands systematic trade-offs among RoEA size, energy consumption, and other system performance, with the optimal solution adjusted case by case.

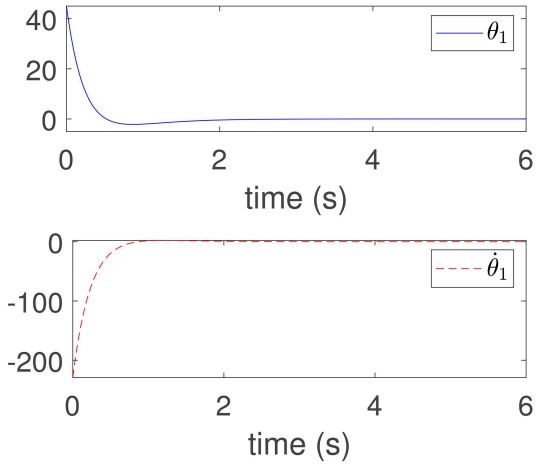

Figure 16 (Color online) The curves of θ_1 and $\dot{\theta}_1$ of the system (6).

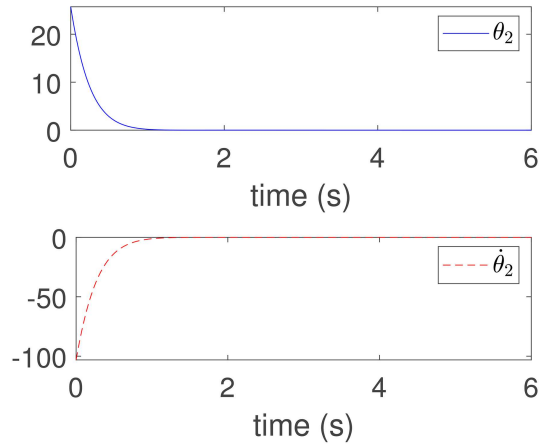

Figure 17 (Color online) The curves of θ_2 and $\dot{\theta}_2$ of the system (6).

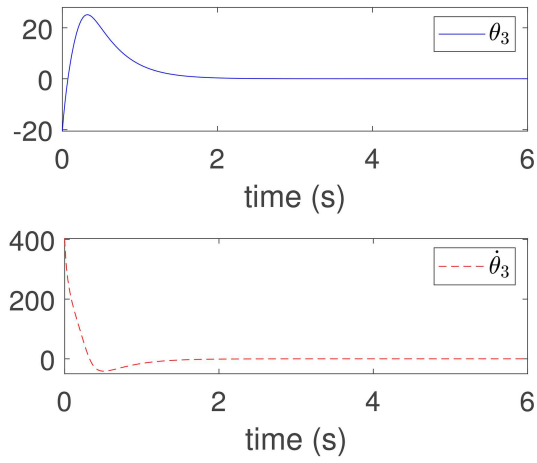

Figure 18 (Color online) The curves of θ_3 and $\dot{\theta}_3$ of the system (6).

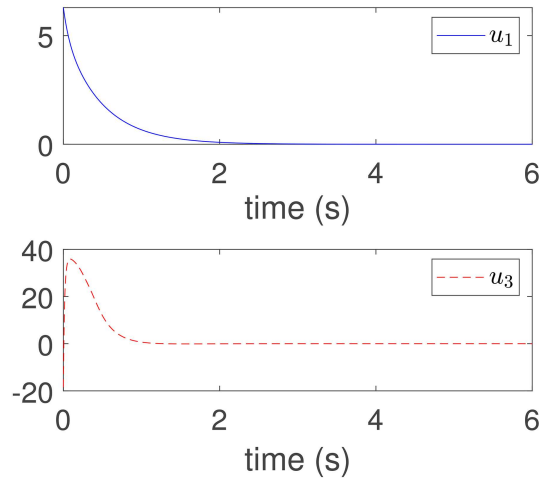

Figure 19 (Color online) The curves of u_1 and u_3 of the system (6).

7 Conclusion

In this paper, we have addressed the substabilization problem for a class of CIPSs with individual control input failure. In order to design controllers, the original CIPS is converted into a sub-FAS model. For the obtained sub-FAS, the FAS approach is utilized to design the corresponding substabilizing controllers within the feasible set. Further, the RoEA is derived, in which the closed-loop sub-FAS is exponentially stable, and the original CIPS exhibits good system performance. Simulation results prove the effectiveness of the proposed control method. In fact, input failure frequently occurs in other real-world systems as well, such as robotic systems and UAV systems. Therefore, in future work, we are interested in further investigating the substabilization problems for such systems.

Acknowledgements This work was supported by Science Center Program of National Natural Science Foundation of China (Grant No. 62188101), Guangdong Provincial Key Laboratory of Fully Actuated System Control Theory and Technology (Grant No. 2024B1212010002), Shenzhen Key Laboratory of Control Theory and Intelligent Systems (Grant No. ZDSYS20220330161800001), and Shenzhen Science and Technology Program (Grant No. KQTD20221101093557010).

References

1 Duan G R. High-order system approaches: I. Fully-actuated systems and parametric designs (in Chinese). Acta Autom Sin, 2020, 46: 1333–1345
2 Duan G R. High-order fully actuated system approaches: part IV. Adaptive control and high-order backstepping. Int J Syst Sci, 2021, 52: 972–989
3 Cai M, He X, Zhou D. Fault-tolerant tracking control for nonlinear observer-extended high-order fully-actuated systems. J Franklin Institute, 2023, 360: 136–153
4 Cai M, He X, Zhou D H. High-order fully actuated systems: tolerating multiplicative actuator faults. In: Proceedings of CAA Symposium on Fault Detection, Supervision and Safety for Technical Processes, 2023

5 Cai M, He X, Zhou D. Low-power fault-tolerant control for nonideal high-order fully actuated systems. IEEE Trans Syst Man Cybern Syst, 2023, 53: 4875–4887
6 Cai M, He X, Zhou D. Unknown nonaffine high-order fully actuated systems: trajectory tracking and fault tolerance. IEEE Trans Syst Man Cybern Syst, 2024, 54: 3854–3864
7 Gong M, Sheng L, Zhou D. Robust fault-tolerant stabilisation of uncertain high-order fully actuated systems with actuator faults. Int J Syst Sci, 2024, 55: 2518–2530
8 Ma Y H, Zhang K, Jiang B. Prescribed-time fault-tolerant control for fully actuated heterogeneous multiagent systems: a hierarchical design approach. IEEE Trans Aerosp Electron Syst, 2023, 59: 6624–6636
9 Ma Y, Zhang K, Jiang B. Neuroadaptive cooperative fault-tolerant control of heterogeneous multiagent systems based on fully actuated system approaches. IEEE Trans Cybern, 2024, 54: 4581–4592
10 Irfan S, Zhao L, Ullah S, et al. Control strategies for inverted pendulum: a comparative analysis of linear, nonlinear, and artificial intelligence approaches. Plos One, 2024, 19: e0298093
11 Lozano R, Fantoni I, Block D J. Stabilization of the inverted pendulum around its homoclinic orbit. Syst Control Lett, 2000, 40: 197–204
12 Lee J, Mukherjee R, Khalil H K. Output feedback stabilization of inverted pendulum on a cart in the presence of uncertainties. Automatica, 2015, 54: 146–157
13 El-Bardini M, El-Nagar A M. Interval type-2 fuzzy PID controller for uncertain nonlinear inverted pendulum system. ISA Trans, 2014, 53: 732–743
14 Ullah S, Khan Q, Mehmood A, et al. Robust backstepping sliding mode control design for a class of underactuated electro–mechanical nonlinear systems. J Electr Eng Technol, 2020, 15: 1821–1828
15 Eremin E L, Nikiforova L V, Shelenok E A. Combined nonlinear control of a system of inverted pendulums with control signal constraints. Optoelectron Instrument Proc, 2021, 57: 396–405
16 Attia M S, Bouafoura M K, Benhadj Braiek N. A near-optimal decentralized control approach for polynomial nonlinear interconnected systems. Trans Institute Measurement Control, 2021, 43: 1363–1375
17 Feydi A, Elloumi S, Jammazi C, et al. Decentralized finite-horizon suboptimal control for nonlinear interconnected dynamic systems using SDRE approach. Trans Institute Measurement Control, 2019, 41: 3264–3275
18 Yoo S J, Park J B, Choi Y H. Decentralized adaptive stabilization of interconnected nonlinear systems with unknown non-symmetric dead-zone inputs. Automatica, 2009, 45: 436–443
19 Hu L Y, Duan G R. Adaptive guaranteed cost tracking control for high-order nonlinear systems based on fully actuated system approaches. Trans Institute Measurement Control, 2024, 46: 1283–1295
20 Zhang L, Zhu L, Hua C. Practical prescribed time control based on high-order fully actuated system approach for strong interconnected nonlinear systems. Nonlinear Dyn, 2022, 110: 3535–3545
21 Hmidi R, Ben Brahim A, Dhahri S, et al. Sliding mode fault-tolerant control for Takagi-Sugeno fuzzy systems with local nonlinear models: Application to inverted pendulum and cart system. Trans Institute Measurement Control, 2021, 43: 975–990
22 Zeghlache S, Ghellab M Z, Djerioui A, et al. Adaptive fuzzy fast terminal sliding mode control for inverted pendulum-cart system with actuator faults. Math Comput Simul, 2023, 210: 207–234
23 Alruwaily Y, Kharrat M. Funnel-based adaptive neural fault-tolerant control for nonlinear systems with dead-zone and actuator faults: application to rigid robot manipulator and inverted pendulum systems. Complexity, 2024, 2024: 1–13
24 Guo T, Xiong J. A new global fuzzy fault-tolerant control for a double inverted pendulum based on time-delay replacement. Neural Comput Applic, 2018, 29: 467–476
25 Zhang J X, Yang G H. Prescribed performance fault-tolerant control of uncertain nonlinear systems with unknown control directions. IEEE Trans Automat Contr, 2017, 62: 6529–6535
26 Mao Z, Jiang B, Shi P. Fault-tolerant control for a class of nonlinear sampled-data systems via a Euler approximate observer. Automatica, 2010, 46: 1852–1859
27 Wang M, Zhou D. Fault tolerant control of feedback linearizable systems with stuck actuators. Asian J Control, 2008, 10: 74–87
28 Yang J Z, Zhang J X, Chai T. Low-complexity decentralized output-feedback fault-tolerant control of general unknown interconnected nonlinear systems. IEEE Trans Automat Sci Eng, 2025, 22: 5852–5862
29 Guo B, Dian S, Zhao T. Event- driven-observer-based adaptive distributed sliding mode fault compensation control for interconnected nonlinear systems. Int J Robust Nonlinear Control, 2024, 34: 2013–2035
30 Duan G R. Substability and substabilization: control of subfully actuated systems. IEEE Trans Cybern, 2023, 53: 7309–7322
31 Duan G R. Fully actuated system approach for control: an overview. IEEE Trans Cybern, 2024, 54: 7285–7306